Chemical strain-dependent two-dimensional transport at RAlO_{3}/SrTiO_{3} interfaces (R=La,Nd,Sm,and Gd)

Chen Li, Xuan Shen, Yurong Yang, Yuhang Bai, Zhoushen Yuan, Dong Su, Aidong Li, Shantao Zhang, Peng Wang, Laurent Bellaiche, and Di Wu

Phys. Rev. B **94**, 241116 — Published 27 December 2016

DOI: 10.1103/PhysRevB.94.241116

Chemical strain-dependent 2-dimensional transport at ReAlO$_3$/SrTiO$_3$ (Re=La, Nd, Sm and Gd) interfaces

Chen Li,[1] Xuan Shen,[1] Yurong Yang,[2,*] Yuhang Bai,[1] Zhoushen Yuan,[1] Dong Su,[3] Aidong Li,[1] Shantao Zhang,[1] Peng Wang,[1] Laurent Bellaiche,[2] and Di Wu[1,†]

[1]*National Laboratory of Solid State Microstructures, Department of Materials Science and Engineering, College of Engineering and Applied Sciences, and Collaborative Innovation Center of Advanced Microstructures, Nanjing University, Nanjing 210093, China*

[2]*Department of Physics and Institute for Nanoscience and Engineering, University of Arkansas, Fayetteville, Arkansas 72701, USA*

[3]*Center for Functional Nanomaterials, Brookhaven National Laboratory, Upton, New York 11973, USA*

(Dated: November 22, 2016)

Abstract

Perovskite ReAlO$_3$ (Re=La, Nd, Sm and Gd) films have been deposited epitaxially on (001) TiO$_2$-terminated SrTiO$_3$ substrates. It is observed that the 2-dimensional transport characteristics at the ReAlO$_3$/SrTiO$_3$ interfaces are very sensitive to the species of rare-earth element, that is to *chemical* strain. Although electron energy loss spectroscopy measurements show that electron transfer occurs in all the four polar/non-polar heterostructures, the amount of electrons transferred across SmAlO$_3$/SrTiO$_3$ and GdAlO$_3$/SrTiO$_3$ interfaces are much less than those across LaAlO$_3$/SrTiO$_3$ and NdAlO$_3$/SrTiO$_3$ interfaces. First-principles calculations reveal the competition between ionic polarization and electronic polarization in the polar layers in compensating the build-in polarization due to the polar discontinuity at the interface. In particular, a large ionic polarization is found in SmAlO$_3$/SrTiO$_3$ and GdAlO$_3$/SrTiO$_3$ systems (which experience the largest tensile epitaxial strain), hence reducing the amount of electrons transferred.

PACS numbers: 68.37.Og, 71.10.Ca, 31.15.A-, 79.60.Jv

In the last decade, emerging phenomena in complex oxide heterostructures have attracted great interest.[1] For example, a 2-dimensional electron gas (2DEG) has been observed on the interface of two insulating oxides, $LaAlO_3$ (LaAO) and $SrTiO_3$ (STO).[2] A variety of intriguing properties on the LaAO/STO interface, such as superconductivity[3,4], magnetoresitance[5,6], ferromagnetism[7–9] and even electromechanical responses[10], have been reported, providing opportunities for the development of future oxide electronic devices. For instance, Cen *et al.* demonstrated a field effect device using the LaAO/STO channel.[11,12] Non-volatile memory functions have been observed in this kind of field effect device by using a ferroelectric gate[13,14] or surface charge injection.[15] Furthermore, surface charges and chemical adsorbates have been found to have a significant influence on the 2-dimentional transport.[16,17] Sensors for polar molecules and gas detectors have been achieved based on this effect.[18,19]

Although the transport characteristics of metallic LaAO/STO interfaces have been studied theoretically and experimentally for years,[2,3,20,21] the physical origin of the interface conductivity is still under debate.[22] It has originally been ascribed to 'polar catastrophe' on the LaAO/STO polar/non-polar interface[23]. However, electron doping by oxygen vacancies in STO,[24–26] cation intermixing across the interface[27] and non-stoichiometry in LaAO[28,29] have also been used to explain the 2-dimensional transport on the LaAO/STO interface. In the 'polar catastrophe' scenario, the electrostatic energy increases with the increase of LaAO thickness, due to the interface polar discontinuity.[23] This imposes a transfer of electrons from the LaAO layer into the empty conduction band of the STO substrate when the LaAO thickness is above 4 unit cells (u.c.).[2,23] However, Hamann *et. al.* pointed out that ionic reconstruction (polar lattice distortion) may relieve the electrostatic energy accumulation and retard the electron reconstruction.[30,31] Therefore, strain, which couples with ionic polar distortions, may play an important role on the interfacial reconstruction, and hence, the 2-dimensional transport – as, e.g., evidenced by the fact that the LaAO/STO interface is insulating under tensile strain.[32].

In this study, we systemically investigate the effect of chemical strain (i.e., different rare-earth elements) on the 2-dimensional transport at the interface of $ReAlO_3$ (ReAO, Re=La, Nd, Sm and Gd) and TiO_2-terminated STO. All ReAO materials are band insulators in bulk.[33] Similar to LaAO/STO, all of the other three ReAO/STO heterostructures can also be regarded as an alternate stacking of charged $(ReO)^+$ and $(AlO_2)^-$ on neutral $(TiO_2)^0$

and $(SrO)^0$ layers. According to the 'polar catastrophe' scenario, electron transfer should occur at all these four polar/non-polar interfaces. However, we observe that electrons transferred into interfacial Ti 3*d* orbitals in SmAO/STO and GdAO/STO are less than those in LaAO/STO and NdAO/STO. First-principles calculations reveal that chemical strain has a great impact on lattice distortions in the polar overlayer, which influences the electrostatic energy accumulated and the amount of electrons transferred.

The *Re*AO layers were deposited on TiO_2-terminated (001) STO substrates by pulsed laser deposition monitored *in situ* by reflective high energy electron diffraction (RHEED). The (001) STO substrates were treated by etching with buffered hydrofluoric acid in an ultrasonic bath, followed by annealing in flowing O_2 at 950 ^{0}C for 60 min, similar to the procedure described by Koster and coworkers.[34] Laser ablation was performed using the 248 nm radiation from a KrF excimer laser (Compex Pro 205 F, Coherent) at a repetition rate of 2 Hz. The laser energy density on the *Re*AO ceramic target was estimated as about 1.8$\sim$2.2 J/cm^2. During deposition, the substrate temperature and the oxygen chamber pressure were maintained at 750 ^{0}C and 10^{-3} mbar, respectively. The thickness of *Re*AO was controlled by counting the intensity oscillations of the specular spot in the RHEED pattern. High resolution X-ray diffraction (XRD) was performed at BL14B1 beam line of Shanghai Synchrotron Radiation Facility. The surface morphology of the heterostructures was checked by an Asylum Research Cypher-ES atomic force microscope (AFM). Cross-sectional specimens for transmission electron microscopy were prepared by 'lift-out' using a focused ion beam system (Helios, FEI). Scanning transmission electron microscopy (STEM) images, collected using a high-angle annular dark field detector, and electron energy loss spectroscopy (EELS) characterizations were performed using a probe aberration-corrected Hitachi HD2700C dedicated STEM operating at 200 kV, with a nominal spatial resolution of 0.9 Å. Transport properties were measured with a Quantum Design physical property measurement system (PPMS-9) in Van-der-Pauw geometry through aluminum electrical contacts to the *Re*AO/STO interface, achieved by direct wire bonding (7476D, West Bond). Interface sheet carrier density was obtained from Hall measurement by scanning a magnetic field from -0.2 to 0.2 T then back to -0.2 T.

The surface of *Re*AO films show a clear step-and-terrace structure. XRD patterns recorded around the (002) reflection of STO substrates show only (002) diffraction peaks from the *Re*AO layers with thickness fringes. Cross-sectional STEM images show atomically

abrupt interfaces in all the samples, in absence of interfacial dislocations. EELS line-scans across the *Re*AO/STO interfaces show that the transmission layers in *Re*AO/STO are less than 1 nm. These results demonstrates the high quality of *Re*AO/STO epitaxy.[35]

Figure 1(a) shows the sheet resistance as a function of temperature for LaAO/STO, NdAO/STO, SmAO/STO and GdAO/STO interfaces, in which all the *Re*AO overlayers are of 10 u.c. in thickness. It is clear that both LaAO/STO and NdAO/STO heterostuctures exhibit room-temperature metallic interfaces with the sheet resistance decreasing with decreasing temperature. The sheet resistance of the two metallic interfaces shows a slight upturn at low temperatures, which may be ascribed to variable range hopping transport due to carrier localization.[36] For the NdAO/STO interface, the larger tensile strain may cause a stronger localization, which limits the carrier mobility and thus results in the clear low-temperature resistance upturn observed. Hall coefficients obtained from these two metallic interfaces are negative, revealing that the dominant carriers at both interfaces are electrons. This is consistent with previous reports for LaAO and NdAO deposited on TiO_2-terminated STO substrates.[21,36] The mobility and density of the interfacial electrons are shown in Fig. 1(b). The values of carrier mobility and sheet carrier density at 7 K are 2.9×10^{13} e/cm^2 and 520 cm^{2}V^{-1}s^{-1} for LaAO/STO and 1.5×10^{13} e/cm^2 and 1.4 cm^{2}V^{-1}s^{-1} for NdAO/STO, similar to those reported previously.[21,36] In contrast, the two interfaces with heavier *A* site rare-earth elements in the aluminate overlayer, SmAO/STO and GdAO/STO, are both insulating. As shown in Fig. 1(a), the sheet resistances are 5-6 orders higher than those of metallic LaAO/STO and NdAO/STO interfaces at room temperature and increases rapidly with decreasing temperature to values beyond the measurement capability of our facilities ($\sim 10^{13}$ $\Omega/\Box$).

According to the 'polar catastrophe' scenario,[2] all the *Re*AO/STO interfaces might be metallic because electrons should be transferred into the empty Ti 3*d* orbitals at the interface to avoid the dispersion of electrostatic potential as a result of interface polar discontinuity. To explain the difference in *Re*AO/STO interfacial transport characteristics, we then probe the filling of Ti 3*d* orbitals using subtle changes in the fine structure of the EELS Ti-$L_{2,3}$ edge as an indicator. Abbate *et. al.*[37] observed, in soft X-ray absorption spectra, that the valley between Ti $2p_{1/2}\rightarrow3d_{t_{2g}}$ and Ti $2p_{1/2}\rightarrow3d_{e_g}$ components vanishes as more and more electrons are doped into Ti 3*d* orbitals. Verbeeck *et. al.*[38] have observed a reduction of the valley in LaAO/STO heterostructures by comparing the spectrum acquired well within

the STO substrate with the one acquired from the interface. Figure 2 shows the Ti-$L_{2,3}$ EELS spectra collected from atomic layers across the *Re*AO/STO interface. Regarding the STEM image of GdAO/STO in Fig. 2 (e) as an example, the number labeled on each spectrum indicates the distance of the atomic layer from the interface, which is labeled with '0'. Spectra with negative numbers are taken from inside the STO substrate and those with positive numbers are taken from within the *Re*AO overlayer. For all the four *Re*AO/STO heterostructures, there is a clear valley between the Ti $2p_{1/2}\rightarrow 3d_{t_{2g}}$ and Ti $2p_{1/2}\rightarrow 3d_{e_g}$ components inside the STO substrate. This is consistent with the empty Ti $3d$ orbitals in STO. For LaAO/STO and NdAO/STO interfaces, as shown in Figs. 2 (a) and (b) respectively, the valley reduces as the electron probe approaches close to the interface from the STO side. This indicates the filling of Ti $3d$ orbitals. However, for SmAO/STO and GdAO/STO interfaces, as shown in Fig. 2 (c) and (d) respectively, clear valleys can still be observed in the spectra taken from the interface. Comparison of the normalized EELS fine structure of these four *Re*AO/STO heterostructures are shown in Fig. 2 (f). It is clear that, compared with LaAO/STO and NdAO/STO interfaces, Ti $3d$ spectra acquired from SmAO/STO and GdAO/STO interfaces are closer to that acquired from STO interior. The electron reconstruction, which moves electrons from the O $2p$ orbitals in the polar overlayers into the interfacial Ti $3d$ orbitals,[21,39] occurs in SmAO/STO and GdAO/STO. However, the transferred electrons are less than those in LaAO/STO and NdAO/STO interfaces. The Ti-$L_{2,3}$ core level shift to lower energy is also an indicator of the reduced Ti ions. It is indeed observed. In LaAO/STO and NdAO/STO, the spectra acquired from interfacial Ti is shifted about 0.4∼0.5 eV from those inside the STO substrate, while the shift is only 0.1∼0.2 eV in SmAO/STO and GdAO/STO.[35] This again indicates that less electrons are transferred in the latter case. Comparisons between EELS spectra of O-K edges acquired from inside the STO substrate and from various *Re*AO/STO interfaces lead to the same conclusion.[35]

Let us try to understand these effects. For that, it is important to reiterate that, in *Re*AO/STO heterostructures, *Re*AO layers contain oppositely charged $(ReO)^{+1}$ and $(AlO_2)^{-1}$ layers.[40,41] This yields a build-in polarization P^0_{ReAO}=e/2a^2 in *Re*AO layers along the [001] direction, where a is the in-plane lattice constant and e the electronic charge. In contrast, the build-in polarization is zero in STO substrate because of neutral $(SrO)^0$ and $(TiO_2)^0$ layers. Polarization in the two sides of the heterointerfaces is discontinuous. As

discussed in the literature,[39,40], this polarization discontinuity between the STO and *Re*AO layers can be compensated by two different mechanisms that are not mutually exclusive: (1) electrons on the *Re*AO surface may transfer to the *Re*AO/STO interface, which is usually coined as an electronic reconstruction and that provides a charge density denoted as σ^e here in the interface; and (2) the *Re*AO layers may adopt ionic distortions, which generates a polarization along the growth direction, termed as P^i, which can be estimated from the Born effective charge tensor and the atomic displacements.[35] As a result, we have:

$$P^0_{ReAO} = \frac{e}{2a^2} = \sigma^e + P^i. \quad (1)$$

σ^e and P^i are competitive mechanisms to compensate the build-in polarization P^0_{ReAO}. In one limit, $\sigma^e = 0$ (no electrons are transferred from the surface to the interface), the ionic polarization P^i fully compensates the built-in polarization P^0_{ReAO}. This happens when the number of *Re*AO layers n$\leq$3, as reported in both experiments and first-principles calculations for the insulating LaAO/STO interface.[31,39–43] In the opposite limit of infinite *Re*AO thickness, σ^e=P^0_{ReAO}=e/2a^2 (corresponding to a metallic interface with an interfacial carrier density of 3.3×10^{14} e/cm^2), and there is no polar ionic distortion in *Re*AO layers. With the increase of *A*-site atomic number, the lattice mismatch between *Re*AO and STO increases from 2.9 % in LaAO/STO to 4.5 % in GdAO/STO. The large epitaxial strain in ultrathin SmAO and GdAO overlayers may have a great impact on the lattice distortion and P^i, and hence, on σ^e, the density of electrons transferred.[44]

In order to determine the amount of electronic reconstruction and polar ionic polarization in *Re*AO/STO heterostructures, $(ReAO)_5/(STO)_9$ model heterostructures are investigated in the framework of first-principles calculations.[35] *Re*AO/STO heterostructures with thinner *Re*AO layers were also studied. It is observed that the interfaces are metallic when *Re*AO is thicker than 3 u.c. for *Re*=La, Nd, and Sm, and 4 u.c. for *Re*=Gd. We focus on $(ReAO)_5/(STO)_9$ for the calculations because transport measurements generate identical results on $(ReAO)_{10}$/STO and $(ReAO)_5$/STO heterostructures. The details of the model heterostructures and calculation parameters can be found in the Supplemental Material.[35] Figure 3 reports the local density of states (LDOS) of STO layers and the cation-oxygen rumpling in *Re*AO layers in $(ReAO)_5/(STO)_9$. As shown in Fig. 3 (a), electron transfer from the *Re*AO surface to the *Re*AO/STO interface occurs in all the four *Re*AO/STO heterostructures. The resulted σ^e can be computed by summing up the LDOS on all the atoms

of STO integrated from the conduction band minimum up to the Fermi energy. As shown in Fig. 3 (b), all the *Re*AO layers show distinct cation-oxygen rumpling, indicating obviously ionic compensation to the built-in polarization P^0_{ReAO} due to the polar discontinuity at the interface.[41]

Table I summarizes the interface electron density σ^e, the ionic polarization P^i and average out-of-plane lattice constant c of *Re*AO in *Re*AO/STO heterostructures obtained from first-principles calculations. It is clear that σ^e decreases with *Re* going from La to Gd (with increasing tensile strain in polar *Re*AO overlayers). The carrier densities, derived from first-principles calculations, for LaAO/STO ($0.110e/a^2$=7.2×10^{13} e/cm^2) and NdAO/STO ($0.092e/a^2$=6.1×10^{13} e/cm^2) are close to the values measured experimentally (see Fig. 1). Furthermore, the computed transferred electrons in SmAO/STO and GdAO/STO are much less than those in LaAO/STO and NdAO/STO, in agreement with EELS results in Fig. 2. Bark *et al.*[32] pointed out that a large tensile strain may result in defects in LaAO/STO heterostructures, and these defects, as reported, may limit the electron mobility at LaAO/STO interfaces.[40,45] Therefore, defects formed due to the large tensile strain in SmAO/STO and GdAO/STO interfaces may play a role on the insulating behavior observed.

Interestingly and as shown in Table I the ionic polarization P^i increases with *Re* going from La to Gd, as the tensile strain in polar *Re*AO overlayers increases (note that the P^i may be underestimated by the calculated Born effective charge tensor). This is in drastic contrast with cases of typical (001) ferroelectric films, such as $BaTiO_3$, $PbTiO_3$, and $BiFeO_3$, in which the out-of-plane polarization decreases with the increase of tensile strain.[46–49] To further understand this increase of P^i in $(ReAO)_5/(STO)_9$, it is informative to recall that one can also write that $P^i = \varepsilon_0\varepsilon_r E$, where ε_r is the dielectric constant and E is the electric field within the *Re*AO layers. For all the $(ReAO)_5/(STO)_9$ supercell we considered, the *Re*AO thickness (5 u.c.) is larger than the critical thickness for charge transfer. Therefore, E decreases as a function of *Re*AO thickness, according to $E = \frac{\Delta}{nce}$,[40] where n is the number of u.c. layers along the growth direction of *Re*AO and Δ is the energy difference between the valence band of *Re*AO and the conduction band of STO – which is also the potential across the *Re*AO layers in *Re*AO/STO, as well as the difference between the band gap of STO and the band offset between STO and *Re*AO. As a result, one has,

$$P^i = \frac{\varepsilon_0\varepsilon_r\Delta}{nce}. \tag{2}$$

Table I reports the values of Δ, as obtained by subtracting the band offset between STO and ReAO (as computed from first principles) from the experimental band gap of STO, for the $(Re\text{AO})_5/(\text{STO})_9$ heterostructures that we considered. One can see that Δ increases when Re goes from La to Gd, which, along with the concomitant decrease of c, explains the increase of P^i in ReAO, with Re going from La to Gd – since ϵ_r is rather similar in the different ReAO materials.[33,50]

Moreover, it is well known that the LaAO/STO interface is metallic only when the LaAO layer thickness exceeds a critical value, 4 u.c. in most reports.[11,51] As shown in Fig. 4, the 4 u.c. LaAO/STO interface is metallic. However, when the top u.c. of the LAO layer is replaced by a u.c. of GdAO, the interface becomes insulating. The large strain in the GdAO layer induces a large ionic rumpling. Therefore, the ionic polarization P^i in the $(\text{GdAO})_1/(\text{LaAO})_3$ composite polar overlayer is stronger than that in $(\text{LaAO})_4$. The large ionic compensation to the build-in polarization retards the electron transfer in the $[(\text{GdAO})_1/(\text{LaAO})_3]$/STO interface. To further verify the chemical strain effect on the interfacial electronic reconstruction, $(\text{La}_{0.5}\text{Gd}_{0.5})\text{AlO}_3$ (LaGdAO) thin films, 10 u.c. in thickness, were deposited on STO and the 2-dimensional transport characteristics of the LaGdAO/STO interface were measured. The lattice constant of LaGdAO is about 3.77 Å, very close to that of NdAO (3.76 Å).[35] Figure 5 shows the sheet resistance, carrier density and mobility of the LaGdAO/STO and NdAO/STO interfaces as functions of temperature. As expected, the transport characteristics of LaGdAO/STO interface is identical to those of NdAO/STO interface, as a result of similar epitaxial strain in LaGdAO and NdAO polar overlayers.

In summary, a series of ReAO (Re=La, Nd, Sm and Gd) thin films, 10 u.c. in thickness, have been deposited on TiO_2-terminated STO substrates. It is observed that LaAO/STO and NdAO/STO interfaces are metallic, whereas SmAO/STO and GdAO/STO interfaces are insulating. TEM characterizations reveal that less electrons are transferred into interfacial Ti $3d$ orbitals in SmAO/STO and GdAO/STO heterostructures, although electron transfer occurs in all the four interfaces. First-principles calculations demonstrate that the ionic polarization increases with increasing Re atomic number in the polar layer. As a consequence, the large ionic compensation to the build-in polarization reduces the amount of electron transferred. The insulating behavior in SmAO/STO and GdAO/STO interfaces may be ascribed to carrier localization or defect scattering. Our results demonstrate, and explain why, chemical strain is an additional and novel handle in the control of properties

at the interface of complex oxides.

This work was sponsored by State Key Program for Basic Research of China (2015CB921203), Natural Science Foundation of China (11374139 and U1431112). Y.Y. and L.B. thank ONR Grant N00014-12-1-1034. We also acknowledge a challenge and a DURIP grants from DoD allowing us the access of supercomputers and clusters, respectively. Some computations were also made possible thanks to the MRI grant 0722625, MRI-R2 grant 0959124, and CI-TRAIN grant 0918970 from NSF. Electron Microscopy work carried out at the Center for Functional Nanomaterials, and National Synchrotron Light Source, Brookhaven National Laboratory, were supported by the U.S. Department of Energy, Office of Basic Energy Sciences, under Contract No. DE-SC0012704. Shanghai Synchrotron Radiation Facility is acknowledged for providing the beam time and technical assistance for XRD.

---

* yyrwater@uark.edu

† diwu@nju.edu.cn

[1] H. Y. Hwang, Y. Iwasa, M. Kawasaki, B. Keimer, N. Nagaosa, and Y. Tokura, Nat. Mater. **11**, 103 (2012).

[2] A. Ohtomo and H. Y. Hwang, Nature (London) **427**, 423 (2004).

[3] N. Reyren, S. Thiel, A. D. Caviglia, L. F. Kourkoutis, G. Hammerl, C. Richter, C. W. Schneider, T. Kopp, A. S. Rüetschi, D. Jaccard, M. Gabay, D. A. Muller, J. M. Triscone, and J. Mannhart, Science **317**, 1196 (2007).

[4] L. Li, C. Richter, J. Mannhart, and R. C. Ashoori, Nat. Phys. **7**, 762 (2011).

[5] A. Brinkman, M. Huijben, M. Van Zalk, J. Huijben, U. Zeitler, J. C. Maan, W. G. Van Der Wiel, G. Rijnders, D. H. A. Blank, and H. Hilgenkamp, Nat. Mater. **6**, 493 (2007).

[6] Ariando, X. Wang, G. Baskaran, Z. Q. Liu, J. Huijben, J. B. Yi, A. Annadi, A. Roy Barman, A. Rusydi, S. Dhar, Y. P. Feng, J. Ding, H. Hilgenkamp, and T. Venkatesan, Nat. Commun. **2**, 188 (2011).

[7] J. A. Bert, B. Kalisky, C. Bell, M. Kim, Y. Hikita, H.Y. Hwang, and K. A. Moler, Nat. Phys. **7**, 767 (2011).

[8] J.-S. Lee, Y. W. Xie, H. K. Sato, C. Bell, Y. Hikita, H. Y. Hwang, and C.-C. Kao, Nat. Mater. **12**, 703 (2013).

[9] S. Banerjee, O. Erten, and M. Randeria, Nat. Phys. **9**, 626. (2013).

[10] C. W. Bark, P. Sharma, Y. Wang, S. H. Baek, S. Lee, S. Ryu, C. M. Folkman, T. R. Paudel, A. Kumar, S. V. Kalinin, A. Sokolov, E. Y. Tsymbal, M. S. Rzchowski, A. Gruverman, and C. B. Eom, Nano. Lett. **12(4)**, 1765 (2012).

[11] C. Cen, S. Thiel, G. Hammerl, C. W. Schneider, K. E. Andersen, C. S. Hellberg, J. Mannhart, and J. Levy, Nat. Mater. **7**, 298 (2008).

[12] J. W. Park, D. F. Bogorin, C. Cen, D. A. Felker, Y. Zhang, C. T. Nelson, C. W. Bark, C. M. Folkman, X. Q. Pan, M. S. Rzchowski, J. Levy, and C. B. Eom, Nat. Commun. **1**, 94 (2010).

[13] S.-I. Kim, D.-H. Kim, Y. Kim, S. Y. Moon, M.-G. Kang, J. K. Choi, H. W. Jang, S. K. Kim, J.-W. Choi, S.-J. Yoon, H. J. Chang, C.-Y. Kang, S. Lee, S.-H. Hong, J.-S. Kim, and S.-H. Baek, Adv. Mater. **25**, 4612 (2013).

[14] V. T. Tra, J.-W Chen, P.-C. Huang, B.-C. Huang, Y. Cao, C.-H. Yeh, H.-J. Liu, E. A. Eliseev, A. N. Morozovska, J.-Y. Lin, Y.-C. Chen, M.-W. Chu, P.-W. Chiu, Y.-P. Chiu, L.-Q. Chen, C.-L. Wu, and Y.-H Chu, Adv. Mater. **25**, 3357 (2013).

[15] Y. W. Xie, C. Bell, Y. Hikita, and H. Y. Hwang, Adv. Mater. **23**, 1744 (2011).

[16] Y. W. Xie, Y. Hikita, C. Bell, and H. Y. Hwang, Nat. Commun. **2**, 294 (2011).

[17] Y. Li and J. J. Yu, J. Phys.: Condens. Matter **25**, 265004 (2013).

[18] K. Au, D. F. Li, N. Y. Chan, and J. Y. Dai, Adv. Mater. **24**, 2598 (2012).

[19] N. Y. Chan, M. Zhao, J. X. Huang, K. Au, M. H. Wong, H. M. Yao, W. Lu, Y. Chen, C. W. Ong, H. L. W. Chan, and J. Y. Dai, Adv. Mater. **26**, 5962 (2014).

[20] J. Nishimura, A Ohtomo, A. Ohkubo, Y. Murakami, and M. Kawasaki, Jpn. J. Appl. Phys. **43**, 1032 (2004).

[21] M. Huijben, G. Rijnders, D. H. A. Blank, S. Bals, S. Van Aert, J. Verbeeck, G. Van Tendeloo, A. Brinkman, and H. Hilgenkamp, Nat. Mater. **5**, 556 (2006).

[22] S. A. Chambers, M. H. Engelhard, V. Shutthanandan, Z. Zhu, T. C. Droubay, L. Qiao, P. V. Sushko, T. Feng, H. D. Lee, T. Gustafsson, E. Garfunkel, A. B. Shah, J.-M. Zuo, and Q. M. Ramasse, Surf. Sci. Rep. **65(10)**, 317 (2010).

[23] N. Nakagawa, H. Y. Hwang, and D. A. Muller, Nat. Mater. **5**, 204 (2006).

[24] G. Herranz, M. Basletić, M. Bibes, C. Carrétéro, E. Tafra, E. Jacquet, K. Bouzehouane, C. Deranlot, A. Hamzić, J.-M. Broto, A. Barthélémy, and A. Fert, Phys. Rev. Lett. **98**, 216803

(2007).

[25] W. Siemons, G. Koster, H. Yamamoto, W. A. Harrison, G. Lucovsky, T. H. Geballe, D. H. A. Blank, and M. R. Beasley, Phys. Rev. Lett. **98**, 196802 (2007).

[26] A. F. Santander-Syro, O. Copie, T. Kondo, F. Fortuna, S. Pailhés, R. Weht, X. G. Qiu, F. Bertran, A. Nicolaou, A. Taleb-Ibrahimi, P. Le Fèvre, G. Herranz, M. Bibes, N. Reyren, Y. Apertet, P. Lecoeur, A. Barthélémy, and M. J. Rozenberg, Nature **469**, 189 (2011).

[27] W. Meevasana, P. D. C. King, R. H. He, S. K. Mo, M. Hashimoto, A. Tamai, P. Songsiriritthigul, F. Baumberger, and Z. X. Shen, Nat. Mater. **10**, 114 (2011).

[28] P. R. Willmott, S. A. Pauli, R. Herger, C. M. Schlepütz, D. Martoccia, B. D. Patterson, B. Delley, R. Clarke, D. Kumah, C. Cionca, and Y. Yacoby, Phys. Rev. Lett. **99**, 155502 (2007).

[29] E. Breckenfeld, N. Bronn, J. Karthik, A. R. Damodaran, S. Lee, N. Mason, and L. W. Martin, Phys. Rev. Lett. **110**, 196804 (2013).

[30] D. R. Hamann, D. A. Muller, and H. Y. Hwang, Phys. Rev. B **73**, 195403 (2006).

[31] S. Okamoto, A. J. Millis, and N. A. Spaldin, Phys. Rev. Lett. **97**, 056802 (2006).

[32] C. W. Bark, D. A. Felker, Y. Wang, Y. Zhang, H. W. Jang, C. M. Folkman, J. W. Park, S. H. Baek, H. Zhou, D. D. Fong, X. Q. Pan, E. Y. Tsymbal, M. S. Rzchowski, and C. B. Eom, Proc. Natl. Acad. Sci. **108**, 4720 (2011).

[33] S.-Y. Cho, I.-T. Kim, and K. S. Hong, J. Mater. Res. **14**, 114 (1999).

[34] G. Koster, B. L. Kropman, G. J. H. M. Rijnders, D. H. A. Blank and H. Rogalla, Appl. Phys. Lett. **73**, 202920 (1998).

[35] See Supplemental Material at [URL will be inserted by APS] for more details about AFM images, XRD patterns, TEM analysis, EELS line-scan data and first-principle calculations.

[36] A. Annadi, A. Putra, A. Srivastava, X. Wang, Z. Huang, Z. Q. Liu, T. Venkatesan, and Ariando, Appl. Phys. Lett. **101**, 231064 (2012).

[37] M. Abbate, F. M. F. de Groot, J. C. Fuggle, A. Fujimori, Y. Tokura, Y. Fujishima, O. Strebel, M. Domke, G. Kaindl, J. van Elp, B. T. Thole, G. A. Sawatzky, M. Sacchi, and N. Tsuda, Phys. Rev. B **44**, 5419 (1991).

[38] J. Verbeeck, S. Bals, A. N. Kravtsova, D. Lamoen, M. Luysberg, M. Huijben, G. Rijnders, A. Brinkman, H. Hilgenkamp, D. H. A. Blank, and G. Van Tendeloo, Phys. Rev. B **81**, 085113 (2010).

[39] R. Pentcheva and W. E. Pickett, Phys. Rev. Lett. **102**, 107602 (2009).

[40] C. Cancellieri, D. Fontaine, S. Gariglio, N. Reyren, A. D. Caviglia, A. Fête, S. J. Leake, S. A. Pauli, P. R. Willmott, M. Stengel, Ph. Ghosez, and J.-M. Triscone, Phys. Rev. Lett. **107**, 056102 (2011).

[41] M. Stengel and D. Vanderbilt, Phys. Rev. B **80**, 241103 (2009).

[42] V. Vonk, M. Huijben, K. J. I. Driessen, P. Tinnemans, A. Brinkman, S. Harkema, and H. Graafsma, Phys. Rev. B **75**, 235417 (2007).

[43] C. Cantoni, J. Gazquez, F. M. Granozio, M. P. Oxley, M. Varela, A. R. Lupini, S. J. Pennycook, C. Aruta, U. Scotti di Uccio, P. Perna, and D. Maccariello, Adv. Mater. **24**, 3952 (2012).

[44] F. Schoofs, M. A. Carpenter, M. E. Vickers, M. Egilmez, T. Fix, J. E. Kleibeuker, J. L. MacManus-Driscoll and M. G. Blamire, J. Phys.: Condens. Matter **25** 175005(6pp) (2013).

[45] F. Gunkel, S. Wicklein, S. Hoffmann-Eifert, P. Meuffels, P. Brinks, M. Huijben, G. Rijnders, R. Waser, and R. Dittmann, Nanoscale, **7**, 1013 (2015).

[46] Z. G. Gui, S. Prosandeev, and L. Bellaiche, Phys. Rev. B **84**, 214112 (2011).

[47] Y. R. Yang, M. Stengel, W. Ren, X. H. Yan, and L. Bellaiche, Phys. Rev. B **86**, 144114 (2012).

[48] Y. R. Yang, W. Ren, M. Stengel, X. H. Yan, and L. Bellaiche, Phys. Rev. Lett. **109**, 057602 (2012).

[49] Y. R. Yang, W. Ren, D. W. Wang, and L. Bellaiche, Phys. Rev. Lett. **109**, 267602 (2012).

[50] R. D. Shannon, J. Appl. Phys. **73**, 348 (1993).

[51] S. Thiel, G. Hammerl, A. Schmehl, C. W. Schneider, and J. Mannhart, Science **313**, 1942 (2006).

FIGURES

FIG. 1. (a) Temperature dependence of interface sheet resistance of 10 u.c. ReAO/STO samples. (b) Carrier mobility and sheet carrier density of 10 u.c. LaAO/STO and NdAO/STO samples as functions of temperature.

FIG. 2. EELS spectrum of Ti-$L_{2,3}$ edge of (a) LaAO/STO, (b) NdAO/STO, (c) SmAO/STO and (d) GdAO/STO samples. The number labeled on each spectrum indicates the distance of the atomic layer from the interface, which is labeled with '0', as indicated in the STEM image of GdAO/STO interface as an example in (e). (f) Normalized EELS spectra of Ti-$L_{2,3}$ at the interface layer of these four ReAO/STO heterostructures and the STO substrate.

FIG. 3. (a) Local density of states in the interface STO layers and (b) cation-oxygen rumpling in ReAO layers in $(Re\mathrm{AO})_5/(\mathrm{STO})_9$ heterostructures.

FIG. 4. 2-dimensional transport characteristics of $[(\mathrm{GdAO})_1/(\mathrm{LaAO})_3]$/STO and $[(\mathrm{LaAO})_4]$/STO heterostructures.

FIG. 5. Sheet resistance (a) and carrier mobility and sheet carrier density (b) of the 10 u.c. LaGdAO/STO interface as functions of temperature, compared with those of the NdAO/STO interface.

TABLES

TABLE I. Interfacial electron density σ (in e/a^2), ionic polarization P^i (in e/a^2) in ReAO layers, average out-of-plane lattice constant c (in Å) in ReAO layers of the $(Re\mathrm{AO})_5/(\mathrm{STO})_9$ heterostructures. Δ represents the potential (in eV) across the ReAO layers.

$(Re\mathrm{AO})_5/(\mathrm{STO})_9$	LaAO	NdAO	SmAO	GdAO
σ^e	0.110	0.092	0.078	0.045
P^i	0.295	0.330	0.370	0.429
c	3.766	3.681	3.649	3.627
Δ	2.84	3.11	3.24	3.54

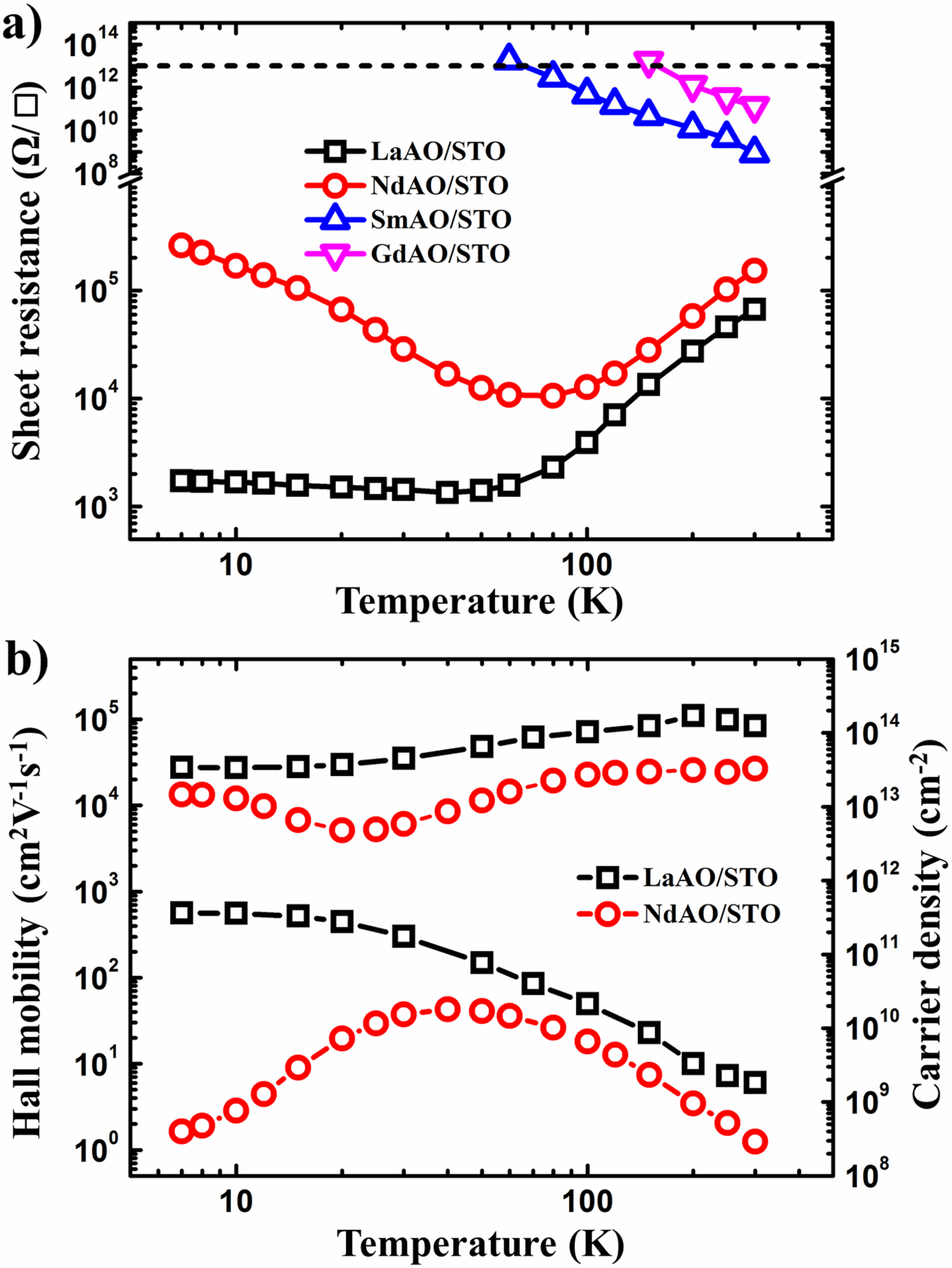
a)
Sheet resistance (Ω/□)
Temperature (K)
LaAO/STO
NdAO/STO
SmAO/STO
GdAO/STO
b)
Hall mobility (cm²V⁻¹s⁻¹)
Carrier density (cm⁻²)
Temperature (K)
LaAO/STO
NdAO/STO

Figure 1

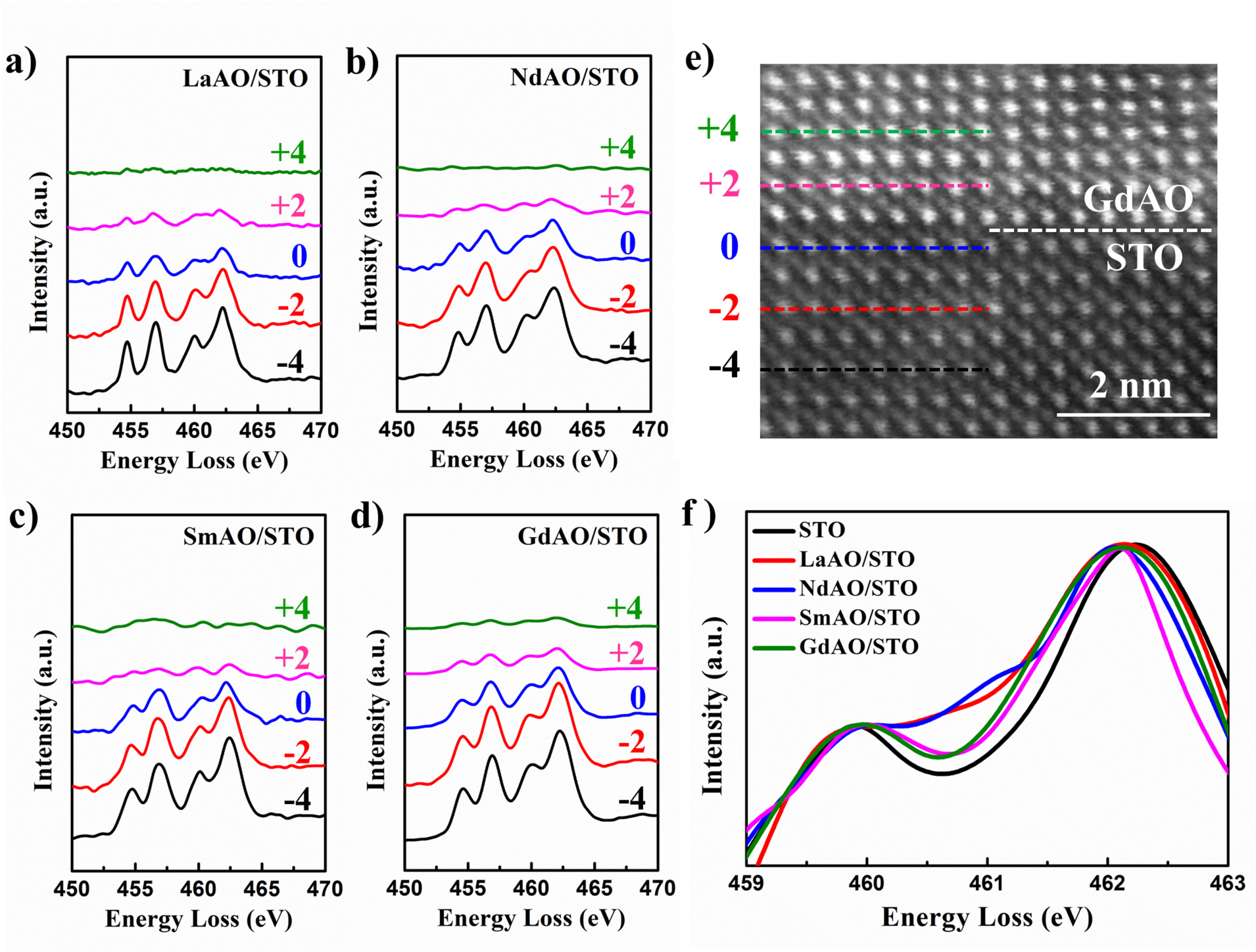
a)
LaAO/STO
+4
+2
0
-2
-4
Intensity (a.u.)
450 455 460 465 470
Energy Loss (eV)
b)
NdAO/STO
+4
+2
0
-2
-4
Intensity (a.u.)
450 455 460 465 470
Energy Loss (eV)
e)
+4
+2
0
-2
-4
GdAO
STO
2 nm
c)
SmAO/STO
+4
+2
0
-2
-4
Intensity (a.u.)
450 455 460 465 470
Energy Loss (eV)
d)
GdAO/STO
+4
+2
0
-2
-4
Intensity (a.u.)
450 455 460 465 470
Energy Loss (eV)
f)
STO
LaAO/STO
NdAO/STO
SmAO/STO
GdAO/STO
Intensity (a.u.)
459 460 461 462 463
Energy Loss (eV)

Figure 2

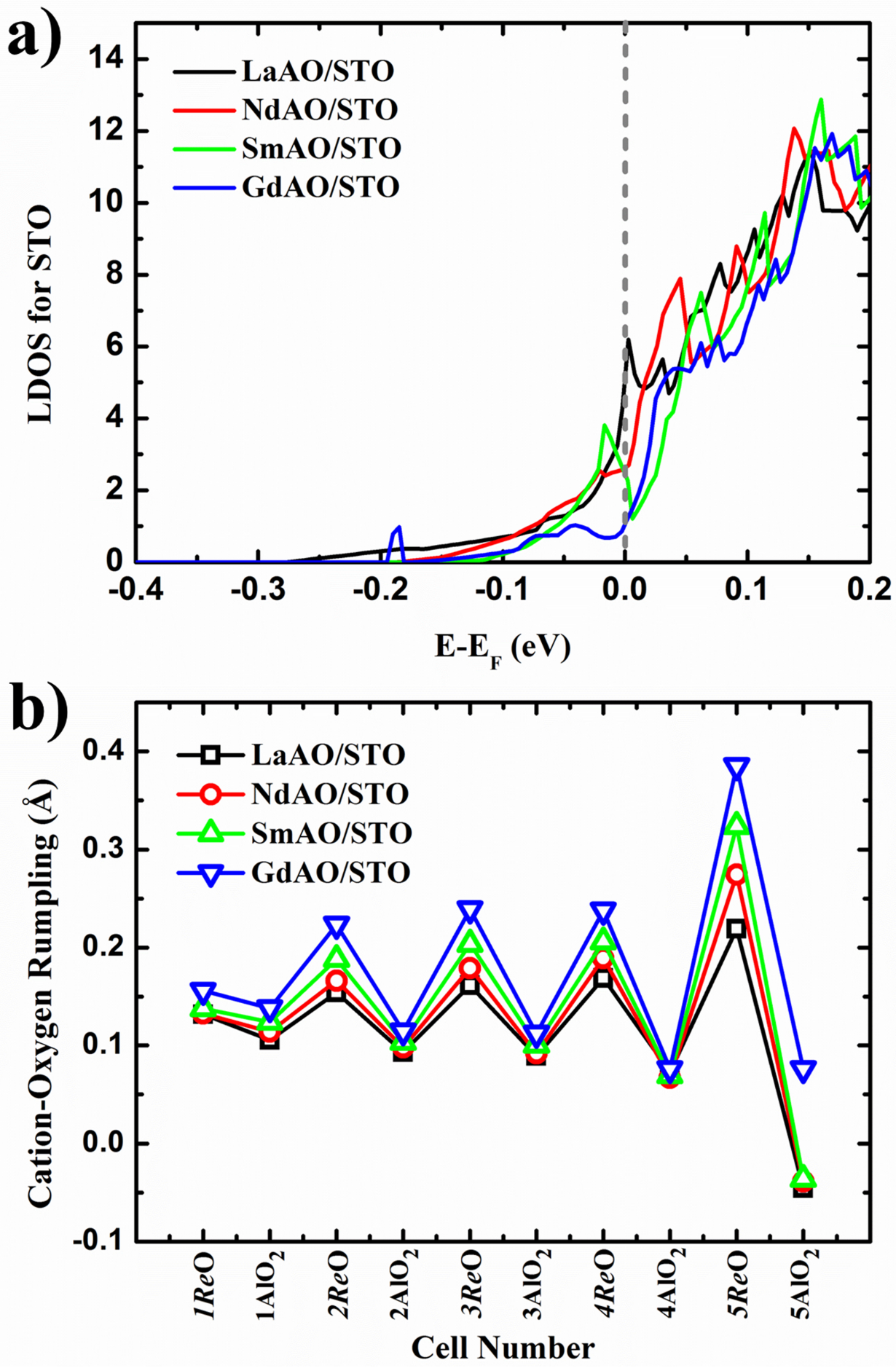
a)
LaAO/STO
NdAO/STO
SmAO/STO
GdAO/STO
LDOS for STO
E-E_F (eV)
b)
LaAO/STO
NdAO/STO
SmAO/STO
GdAO/STO
Cation-Oxygen Rumpling (Å)
1ReO
1AlO2
2ReO
2AlO2
3ReO
3AlO2
4ReO
4AlO2
5ReO
5AlO2
Cell Number

Figure 3

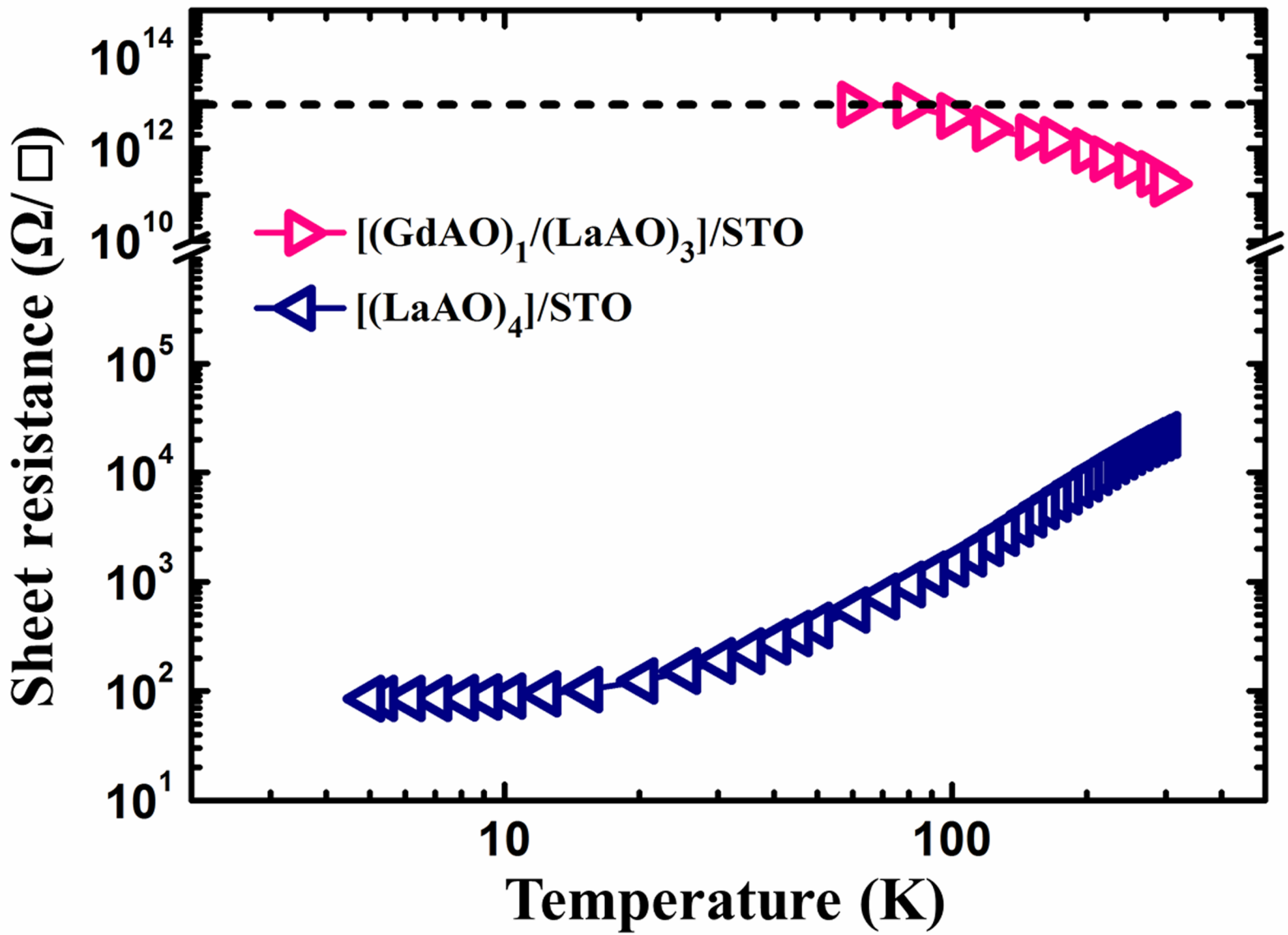
Sheet resistance (Ω/□)
10^14
10^12
10^10
10^5
10^4
10^3
10^2
10^1
[(GdAO)1/(LaAO)3]/STO
[(LaAO)4]/STO
10
100
Temperature (K)

Figure 4

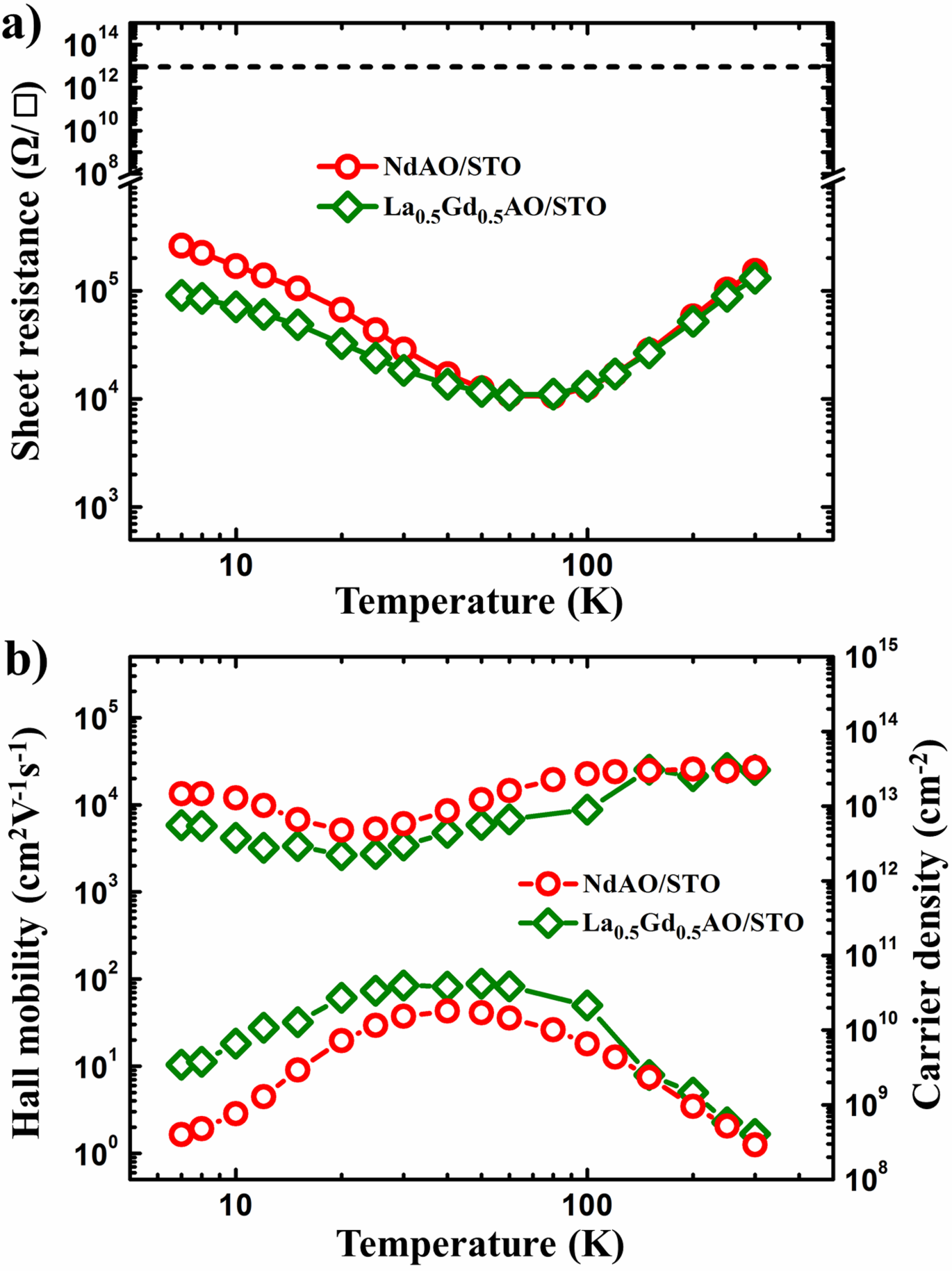
a)
Sheet resistance (Ω/□)
NdAO/STO
La0.5Gd0.5AO/STO
Temperature (K)
b)
Hall mobility (cm2V-1s-1)
Carrier density (cm-2)
NdAO/STO
La0.5Gd0.5AO/STO
Temperature (K)

Figure 5